



HAL
open science

On the early fate of hydrothermal iron at deep-sea vents: A reassessment after in situ filtration

Matthieu Waeles, L. Cotte, B. Pernet-Coudrier, V. Chavagnac, C. Cathalot, T. Leleu, A. Laes-Huon, A. Perhirin, Ricardo D. Riso, P.-M. Sarradin

► To cite this version:

Matthieu Waeles, L. Cotte, B. Pernet-Coudrier, V. Chavagnac, C. Cathalot, et al.. On the early fate of hydrothermal iron at deep-sea vents: A reassessment after in situ filtration. *Geophysical Research Letters*, 2017, 44 (9), pp.4233-4240. 10.1002/2017GL073315 . hal-02613249

HAL Id: hal-02613249

<https://hal.science/hal-02613249>

Submitted on 20 May 2020

HAL is a multi-disciplinary open access archive for the deposit and dissemination of scientific research documents, whether they are published or not. The documents may come from teaching and research institutions in France or abroad, or from public or private research centers.

L'archive ouverte pluridisciplinaire **HAL**, est destinée au dépôt et à la diffusion de documents scientifiques de niveau recherche, publiés ou non, émanant des établissements d'enseignement et de recherche français ou étrangers, des laboratoires publics ou privés.



RESEARCH LETTER

10.1002/2017GL073315

Key Points:

- Deep-sea hydrothermal venting is a major but poorly constrained source of iron to the Ocean
- Iron removal by sulfide precipitation at the early stage of mixing is much more limited than expected in basalt-hosted systems
- Our results have several implications for the quantification of hydrothermal iron fluxes

Supporting Information:

- Supporting Information S1
- Table S1
- Data Set S1

Correspondence to:

M. Waeles and L. Cotte,
waeles@auniv-brest.fr;
laura.cotte@ifremer.fr

Citation:

Waeles, M., L. Cotte, B. Pernet-Coudrier, V. Chavagnac, C. Cathalot, T. Leleu, A. Laës-Huon, A. Perhirin, R. D. Riso, and P.-M. Sarradin (2017), On the early fate of hydrothermal iron at deep-sea vents: A reassessment after in situ filtration, *Geophys. Res. Lett.*, *44*, 4233–4240, doi:10.1002/2017GL073315.






Received 14 MAR 2017

Accepted 26 APR 2017

Accepted article online 28 APR 2017

Published online 9 MAY 2017

On the early fate of hydrothermal iron at deep-sea vents: A reassessment after in situ filtration

M. Waeles¹ , L. Cotte^{1,2}, B. Pernet-Coudrier¹, V. Chavagnac³ , C. Cathalot⁴, T. Leleu³, A. Laës-Huon⁵ , A. Perhirin² , R. D. Riso¹, and P.-M. Sarradin² 

¹Université de Bretagne Occidentale, LEMAR UMR-CNRS 6539, IUEM, Plouzané, France, ²Ifremer, Environnement Profond (DEEP-REM), ZI de la Pointe du Diable, Plouzané, France, ³Laboratoire Géosciences Environnement Toulouse, GET UMR-CNRS 5563, Université de Toulouse, Toulouse, France, ⁴Ifremer, Géochimie et Métallogénie (GM-REM, Plouzané, France), ⁵Ifremer, Laboratoire Détection, Capteurs et Mesures (REM/RDT, Plouzané, France)

Abstract Deep-sea hydrothermal venting is now recognized as a major source of iron (Fe), an essential trace element that controls marine productivity. However, the reactions occurring during dispersal from buoyant plumes to neutrally buoyant hydrothermal plumes are still poorly constrained. Here we report for the first time on the dissolved-particulate partition of Fe after in situ filtration at the early stage of mixing at different hydrothermal discharges, i.e., Lucky Strike (37°N), TAG (26°N), and Snakepit (23°N) on the Mid-Atlantic Ridge. We found that hydrothermal iron is almost completely preserved (>90%) in the dissolved fraction, arguing for low iron-bearing sulfide precipitation of iron in basalt-hosted systems with low Fe:H₂S ratios. This result can only be explained by a kinetically limited formation of pyrite. The small part of Fe being precipitated as sulfides in the mixing gradient (<10%) is restricted to the inclusion of Fe in minerals of high Cu and Zn content. We also show that secondary venting is a source of Fe-depleted hydrothermal solutions. These results provide new constraints on Fe fluxes from hydrothermal venting.

1. Introduction

Assessing the biogeochemical Fe cycle in the ocean and at its interfaces with solid earth is a challenging yet critical task for Earth scientists [Jickells *et al.*, 2005; Lam and Bishop, 2008]. A variety of observations point to a strong role for hydrothermal activity in the marine Fe budget. Fe concentrations in deep waters can be reproduced by numerical modeling only if a hydrothermal source is included [Tagliabue *et al.*, 2010]. Some Fe is vented as stable pyrite nanoparticles [Yücel *et al.*, 2011], while nonsulfide Fe(II) particles and strong organic Fe chelates have been observed in neutrally buoyant plumes [Toner *et al.*, 2009; Hawkes *et al.*, 2013]. Such reactions act to facilitate the dispersion of hydrothermal Fe from vent sources to the broader ocean.

Efforts by the oceanographic community to acquire reliable data on trace elements across the global ocean (e.g., GEOTRACES) have firmly established the crucial role of hydrothermal activity on the marine Fe inventory [Tagliabue, 2014]. Large basin-scale Fe plumes, hundreds to thousands of kilometers in length, have been revealed at almost each section crossing oceanic ridges [Nishioka *et al.*, 2013; Saito *et al.*, 2013; Resing *et al.*, 2015], despite Fe(II) oxidation and Fe(III) particle coagulation kinetics that are thought to be relatively rapid [Massoth *et al.*, 1998; Field and Sherrell, 2000]. Efforts are now needed to better constrain the chemical reactions involving vented Fe much closer to hydrothermal discharges. Owing to the extreme gradients and diversity of emitted fluids in terms of chemical composition and physical structure [German and Von Damm, 2006] (e.g., focused versus diffusive), investigating areas in close proximity to vents is a demanding task. Different approaches have been undertaken to study this dynamic interface, and we recently showed that in situ filtration is required for limiting chemical changes before shipboard sample recovery [Cotte *et al.*, 2015]. By applying these sampling constraints, we examined for the first time the effective dissolved concentrations of Fe (dFe) during early stages of mixing with the aim to better constrain its early reactivity at deep-sea vents.

2. Materials and Methods

As part of three oceanographic cruises on the RV *Pourquoi Pas?* (Momarsat-2014, Momarsat-2015, and Bicosé-2015), we sampled 18 buoyant plumes of several black smokers on the MAR (supporting information Figure S1). Most of them (16) are located at different sites of the Lucky Strike hydrothermal

field (37°N), i.e., Aisics, Y3, Cypress, White Castle, Capelinhos, Sapin, and Montségur (Figure S1b), while the two others are located at TAG (26°N) and Snakepit (23°N). All sampled vents are hosted on basaltic substratum. The Lucky Strike vent field displays a wide variety of emissions [Barreyre *et al.*, 2012] that produces a very thick and large plume [Wilson *et al.*, 1996] compared to a more focused activity at TAG and Snakepit fields. At each of these sites, in situ filtration was performed in the mixing zone using the Pepito sampler [Cotte *et al.*, 2015] deployed on the remotely operated vehicle (ROV) Victor 6000. Table S1 (see supporting information) presents and summarizes position, depth, temperature range, and dilution factor of each collected vent gradient.

In situ filtered samples were obtained after pumping water into 2L-PVC blood bags (Baxter Fenwall, sterile/NP-FP, R4R2041) and using online filtration at 0.45 μm (HATF, Millipore). For each dive, sampling was carried out toward increasing temperatures in order to cover the mixing gradient from the seawater dominated to hydrothermal-dominated part of the buoyant plume. A temperature sensor is attached to the sampler snorkel with real-time temperature reading in the ROV control room on board the research vessel. The cannula of the sampler was first placed at 1 to 2 m above the vent orifice in order to begin the sampling from the coldest part of the mixing gradient. It was then shifted downward within the central part of the buoyant plume until reaching values in the range 100–150°C. Mean temperature measured during each sampling is provided in the supporting information (Data Set S1). Additional details of the sampling system, sampling procedure after sample recovery and washing of the sampling equipment is described elsewhere [Cotte *et al.*, 2015].

Coupled to the PEPITO sampling, in situ measurements of labile sulfides (ΣS) [Le Bris *et al.*, 2000] and iron (Fe(II)) [Sarradin *et al.*, 2005] were performed using chemical miniaturized (CHEMINI) analyzers [Vuillemin *et al.*, 2009]. Both ΣS and Fe(II) measurements are based on colorimetric detection (methylene blue method and ferrozine method, respectively) and flow injection analysis. Both chemical analyzers were calibrated in situ at the beginning and at the end of each dive using Fe(II) and S(-II) stock solutions. The chemical forms being measured in unfiltered water include dissolved species but also some particulate species that are labile enough to react with methylene blue or ferrozine at pH 4.7 (acetate buffer). The intake for the CHEMINI analyzer was also associated with the PEPITO intake and the temperature probe. Hydrothermal solutions were directly pumped without any filtration, and the signal acquisition (~ 3 min) was initiated at the same time as the PEPITO sampling.

Dissolved Fe, Cu, and Zn concentrations (dFe, dCu, and dZn, respectively) and particulate Fe, Cu, and Zn concentrations (pFe, pCu, and pZn, respectively) were determined using sector field inductively coupled plasma (ICP) mass spectrometry (Element 2, ThermoFisher) [Cotte *et al.*, 2015], whereas dissolved Mn concentrations (dMn) were measured by ICP atomic emission spectrometry (Ultima 2, Horiba Jobin Yvon). Precisions (one sigma) were better than 1% for Mn, 3% for Fe, and Cu and 5% for Zn. The procedure describing the digestion of filters and the preparation of solutions and standards for ICP measurements is detailed in Cotte *et al.* [2015]. The various concentrations presented in this study were generally well above detection limits and blanks (including ultrapure water processed in the PEPITO sampler, filter blanks, and digestion blanks) were below detection limits.

High-temperature hydrothermal fluids were sampled by inserting the snorkel of gas-tight titanium syringes into the main chimney at Aisics, Y3, Cypress, White Castle, and Capelinhos vents that were manipulated and triggered by the hydraulic arm of the ROV Victor 6000. At each dive, four gas-tight titanium syringes were triggered per smoker, and time delay between each sampling replicate did not exceed 20 min. The samples were processed immediately on board after the ROV recovery. First, gases were extracted from sampler and transferred into vacuumed stainless steel canisters. The fluid samples were then extracted and filtered through 0.45 μm Millipore filters and split into different aliquots for onshore analysis and stored at 4°C in a cold room. pH and H_2S were measured on board immediately after processing. H_2S concentrations were measured in the solution with an amperometric microsensor (AquaMS, France). Chemical analyses were conducted at the Geosciences Environment Toulouse laboratory with an inductively coupled plasma-atomic emission spectrometer (ICP-AES; Horiba Ultima2) [Besson *et al.*, 2014]. The instrument is calibrated using mono-elemental solutions, multielemental solution, and International Association for the Physical Sciences of the Oceans standard solution. In these samples, Mg concentration was sufficiently low (i.e., in the range 1–3 mM) to accurately estimate the composition of the hydrothermal end-members after extrapolation to zero-Mg (Table 1).

Table 1. End-Member Chemistry of Hydrothermal Fluids at Lucky Strike (this study), Snakepit, and TAG [James and Elderfield, 1996]^a

Vent	Fluid Type	Date of Sampling	Fe (μM)	Mn (μM)	H ₂ S (mM)	pH	Fe:Mn	Fe:H ₂ S
Aisics (main smoker)	Black smoker	27 Jul 2014	457±16	232±2	1.94±0.10	<3.58	1.97	0.24
		13 Apr 2015	522±17	257±1	0.69±0.14	<3.53	2.03	0.76
		24 Apr 2015	459±11	236±2	1.24±0.15	<3.35	1.94	0.37
Y3 (main smoker)	Black smoker	20 Jul 2014	553±9	273±3	1.49±0.03	<3.76	2.03	0.37
		21 Apr 2015	563±5	280±1	0.90±0.11	<3.68	2.01	0.63
Cypress (main smoker)	Clear smoker	26 Jul 2014	544±12	412±5	1.97±0.16	<3.66	1.32	0.28
		15 Apr 2015	575±3	438±6	1.51±0.46	<3.57	1.31	0.38
White Castle (main smoker)	Black smoker	28 Jul 2014	352±21	332±3	2.98±0.08	<3.65	1.06	0.12
		17 Apr 2015	407±21	369±11	1.34±0.35	<3.49	1.10	0.30
Capelinhos (main smoker)	Black smoker	24 Jul 2014	2306±26	489±4	2.26±0.15	<3.29	4.72	1.0
		20 Apr 2015	2494±44	594±12	0.57±0.21	<3.19	4.20	4.4
Snakepit (main smoker)	Black smoker						5.7	0.4
TAG (main smoker)	Black smoker						8.0	1.9

^aConcentrations in hydrogen sulfide (H₂S), Fe, and Mn correspond to extrapolated zero-magnesium concentrations measured in gas-tight titanium syringe samples. Because pH values cannot be extrapolated to zero-magnesium, end-members pH values can only be suggested to be lower than those measured in the collected samples in which acidic hydrothermal fluid was partially mixed with seawater of pH 8.0.

3. Results and Discussion

3.1. Dissolved and Particulate Fe in the Early Mixing Zone

The sampled area within the first 2 m of venting corresponds to a dilution factor of the hydrothermal fluid with deep seawater of 1 to ~100. This dilution factor can be calculated using dissolved dMn (dMn) as a conservative tracer whose removal rate is considerably slower than the emplacement of neutrally buoyant plumes [Field and Sherrell, 2000]. For the various vents examined, a strictly linear relationship was obtained between dissolved Fe (dFe) and dMn (Figure 1 and Table 2), and the dFe:dMn ratios obtained in the mixing zone (Table 2) were not significantly different from the Fe:Mn ratios determined for end-members (Table 1),

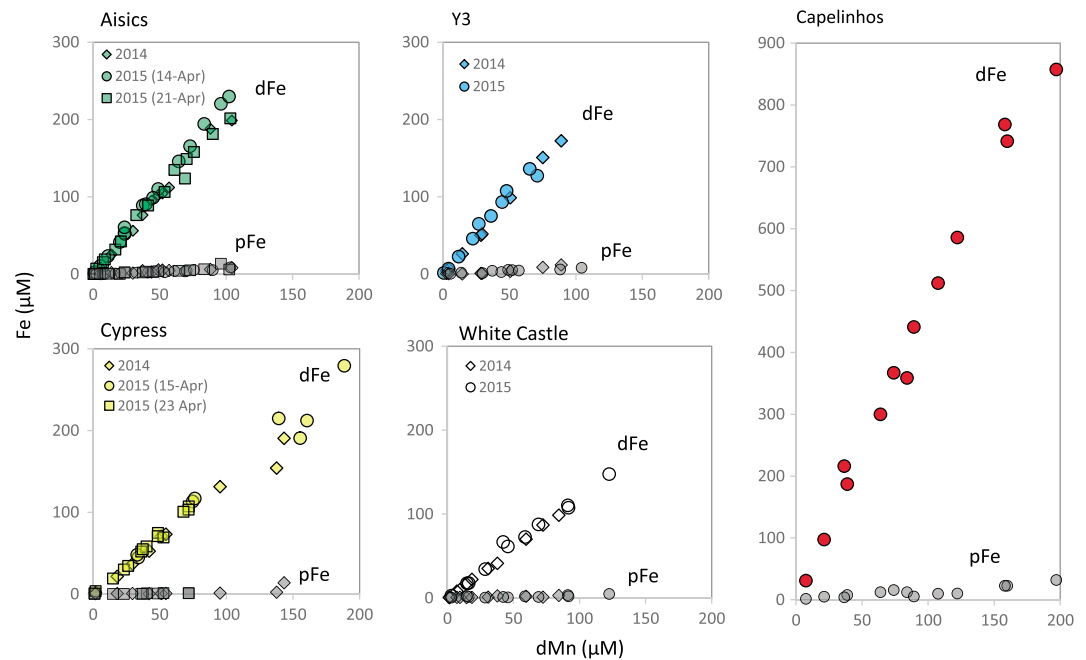


Figure 1. Concentrations of dissolved Fe (dFe) and particulate Fe (pFe) after in situ filtration at several main smokers of the Lucky Strike field. dFe and pFe concentrations are given as a function of dissolved Mn (dMn), a conservative tracer of the mixing of hydrothermal fluids with deep seawater. Error bars are within the symbols. The regression lines for these data are provided in Table 2, and data are given in supporting information (Data Set S1).

Table 2. dFe-dMn and pFe-dMn Relationships in the Mixing Zone of the Various Vents Examined After Regression With the Least Squares Method to the One Parameter Linear $d\text{Fe} = a \times d\text{Mn}$ and $p\text{Fe} = b \times d\text{Mn}$ Models (F Tests Indicated That a Two Parameter Linear Model, i.e., With Slope and Intercept, did not Significantly Increase the R^2)^a

Vent	Fluid Type	Date of Sampling	Dissolved			Particulate			a/(a+b) (%)
			dFe-dMn Relationship (dFe = a × dMn Model)	R^2	n	pFe-dMn Relationship (pFe = b × dMn Model)	R^2	n	
Aisics (main smoker)	Black smoker	26 Jul 2014	dFe = (2.02±0.08) dMn	0.994	10	pFe = (0.08±0.02) dMn	0.92	10	96±7
		14 Apr 2015	dFe = (2.28±0.03) dMn	0.998	16	pFe = (0.08±0.02) dMn	0.77	15	96±3
		21 Apr 2015	dFe = (2.03±0.08) dMn	0.993	15	pFe = (0.07±0.01) dMn	0.93	15	97±7
Y3 (main smoker)	Black smoker	23 Jul 2014	dFe = (1.95±0.06) dMn	0.997	8	pFe = (0.11±0.03) dMn	0.84	8	95±7
		25 Apr 2015	dFe = (2.04±0.14) dMn	0.984	10	pFe = (0.16±0.02) dMn	0.97	9	93±12
Cypress (main smoker)	Clear smoker	22 Jul 2014	dFe = (1.27±0.09) dMn	0.985	9	pFe = (0.04±0.04) dMn	0.31	9	97±15
		15 Apr 2015	dFe = (1.33±0.13) dMn	0.973	9				
		23 Apr 2015	dFe = (1.45±0.04) dMn	0.995	14	pFe = (0.02±0.01) dMn	0.83	10	99±6
White Castle (main smoker)	Black smoker	28 Jul 2014	dFe = (1.17±0.03) dMn	0.998	10	pFe = (0.03±0.02) dMn	0.70	10	97±4
		18 Apr 2015	dFe = (1.23±0.06) dMn	0.991	11	pFe = (0.03±0.01) dMn	0.74	11	97±9
Capelinhos (main smoker)	Black smoker	20 Apr 2015	dFe = (4.65±0.17) dMn	0.993	13	pFe = (0.14±0.03) dMn	0.86	13	97±7
Aisics (auxiliary smoker)	Clear smoker	17 Jul 2014	dFe = (1.48±0.07) dMn	0.993	10				
Aisics-Tempo (diffuse vent)	Diffuse vent	19 Jul 2014	dFe = (0.97±0.03) dMn	0.999	4				
Capelinhos (auxiliary smoker)	Clear smoker	25 Jul 2014	dFe = (4.05±0.26) dMn	0.991	7				
Sapin (main smoker)	Clear smoker	20 Jul 2014	dFe = (0.72±0.02) dMn	0.998	7				
Montségur (main smoker)	Clear smoker	16 Jul 2014	dFe = (0.95±0.09) dMn	0.989	6				
Snakepit (auxiliary smoker)	Black smoker	24 Jan 2014	dFe = (4.30±0.48)*dMn	0.959	10				
TAG (auxiliary smoker)	Black smoker	01 Feb 2014	dFe = (4.7±1.9)*dMn	0.968	3				

^aThe determination of the Fe fraction being preserved as dissolved species upon mixing was deduced from the a/(a+b) ratio. Uncertainties on the a/(a+b) ratio were deduced from confidence intervals at 95% on a and b. Note that the relationships obtained at the main smokers of Aisics, Y3, Cypress, White Castle, and Capelinhos are displayed in Figure 1. The data and parameters of the linear regressions are given in the supporting information (Data Set S1).

meaning that dFe behavior is strictly conservative in the examined gradient. Replicate sampling at a same vent up to a year later (Figure 1 and Table 2) leads unambiguously to the same conclusion.

This result provides new constraints on the time period over which Fe remains in the dissolved form and challenges the paradigm, including recent thermodynamic model simulations [Sander and Koschinsky, 2011], that a large part of hydrothermal iron (i.e., 40–100%) should be precipitated as sulfide particles during the very early stages of mixing with seawater [Mottl and McConachy, 1990; German et al., 1991; Rudnicki and Elderfield, 1993; Field and Sherrell, 2000]. In all cases, the elemental analysis of the filters we recovered after in situ filtration showed that particulate Fe (pFe) concentrations were much lower than dFe concentrations (Figure 1) with pFe accounting only for 5±5% of total Fe when considering the whole pFe data set ($n = 111$).

The vent Fe:H₂S ratio has been proposed as an important factor for controlling the Fe loss by sulfide precipitation [Field and Sherrell, 2000]. Most basalt-hosted systems (e.g., TAG, Snakepit, and EPR vents) present low Fe:H₂S ratios (typically in the range 0.3–1.0 mol mol⁻¹) and are viewed as places where sulfide precipitation is important [Mottl and McConachy, 1990; Field and Sherrell, 2000]. On the other hand, at vents exhibiting high Fe/H₂S ratios, such as those along the Endeavor Ridge segment with ratios >100 mol mol⁻¹, the precipitation of Fe sulfides is negligible [Severmann et al., 2004]. The vents sampled at Lucky Strike display low Fe:H₂S ratios, usually in the range 0.3–1.0 mol mol⁻¹, indicating that other factors limit the production of iron sulfide particles. Indeed, this result can only be explained by (1) slow kinetics of pyrite precipitation as compared to the mixing process and/or (2) a stabilization of iron within <0.45 μm “dissolved” fraction in line with the previous findings that pyrite nanoparticles are pervasive in hydrothermal emissions [Yücel et al., 2011]. Applying the semi-empirical kinetic equations obtained by laboratory studies [Graham and Ohmoto, 1994; Rickard, 1997] to MAR hydrothermal solutions actually leads to a rather slow production of pyrite particles, in the order of 0.1 nM h⁻¹. This rate is negligible considering the mixing time of the studied gradients (on the order of tens of seconds). In addition, the formation of pyrite below 300°C involves an iron monosulfide precursor [Schoonen and Barnes, 1991] for which thermodynamic models predict little production in the mixing gradient [Breier et al., 2012]. The limited production of pyrite particles in the mixing gradient of all Lucky Strike vents is also supported by our in situ measurements with a CHEMINI analyzer [Vuillemin et al., 2009]. Indeed, these measurements indicated that at all sites (e.g., the main smoker of Aisics, Figure 2), iron

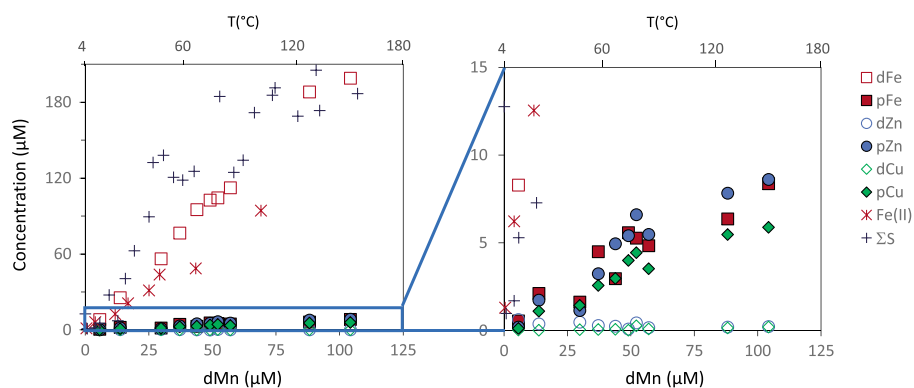


Figure 2. Dissolved and particulate concentrations of Fe, Cu, and Zn (26 July 2014 data) and concentrations of labile sulfide (ΣS) and Fe(II) at the main smoker of Aisics. Concentrations of Fe, Cu, and Zn are summarized in Table S3 (supporting information). ΣS and Fe(II) data (supporting information Table S4) were obtained after in situ measurements with the CHEMINI analyzer and can be plotted as a function of either dissolved Mn or temperature thanks to the linear dMn-T relationship obtained at the main smoker of Aisics (supporting information Figure S3).

occurs essentially as Fe(II) species and coexists with sulfide until the coldest part of the mixing gradient (temperature range 4–20°C, corresponding to a dilution factor of ~ 100 of pure end-member). We propose that the very high preservation of Fe is likely due to the kinetically limited formation of pyrite particles rather than a stabilization of iron under pyrite nanoparticles. This is sustained by pyrite nanoparticles accounting for less than 10% of the filterable iron [Yücel *et al.*, 2011]. We also anticipate that such kinetical control is also prevalent over the whole ascending plume because (1) the rate of pyrite production (0.1 nM h^{-1}) is also negligible considering the mixing time of the whole ascending plume (on the order of tens of minutes) and the dFe concentrations at the emplacement of neutrally buoyant plume ($> 100 \text{ nM}$) [e.g., James and Elderfield, 1996] and (2) Ohnemus and Lam [2015] found no evidence for Fe-sulfide particles in the neutrally buoyant plume of TAG.

3.2. Input of Dissolved Iron From Secondary Venting

The mixing zones of secondary venting, sampled at the base of different main discharges, were characterized by systematically and significantly lower dFe:dMn ratios than those of their relative main black smoker vents (Table 2). At Aisics (Figure S2), dFe:dMn ratios of 1.48 ± 0.07 and 0.97 ± 0.03 were obtained for a clear focused smoker and for the diffusive venting area “Aisics-Tempo.” This is $\sim 30\%$ and $\sim 50\%$ lower than the ratio obtained for the mixing zone of the main black smoker (range 2.0–2.3). In the same manner, the dFe:dMn ratio at Capelinhos auxiliary smoker (4.05 ± 0.26) was below the one found for the main smoker (4.65 ± 0.17). Although we only sample auxiliary smokers at Snakepit and TAG, their dFe:dMn ratios (of 4.3 and 4.7, respectively) also fell below the end-member values of the main smokers reported by James and Elderfield [1996] (5.7 and 8.0, respectively). These results, indicating that secondary venting is a source of Fe depleted hydrothermal solutions, have several implications. First, important iron removals may occur through chemical reactions taking place within the hydrothermal plumbing system prior to venting at auxiliary vents. This includes lower temperatures clear smokers, flanges, cracks, and diffusive sources but constitutes potentially an important source of heat [Barreyre *et al.*, 2012] and Fe [German *et al.*, 2015] on larger spatial scale than localized black smoker discharges. Second, quantification of dissolved Fe fluxes escaping a particular vent field, which is usually done from measurements in the neutrally buoyant plume [e.g., Bennett *et al.*, 2008; Hawkes *et al.*, 2013], must consider the mixing of hydrothermal solutions vented from focused black smokers with Mn-bearing but Fe-depleted solutions from auxiliary venting that are known to be entrained into the same plume [Wilson *et al.*, 1996; Veirs *et al.*, 2006].

3.3. Dissolved-Particulate Partition of Fe as Compared to That of Cu and Zn

As opposed to iron, zinc and copper precipitate quantitatively before venting and/or during the very early stage of mixing ($T > 150^\circ\text{C}$). Indeed, these two metals were mainly found as particulate rather than as dissolved species over the studied gradients. Klevenz *et al.* [2011] and Feely *et al.* [1987] also showed in their studies of particulates phases forming in plumes at 15°N and 5°S MAR and Juan de Fuca Ridge that

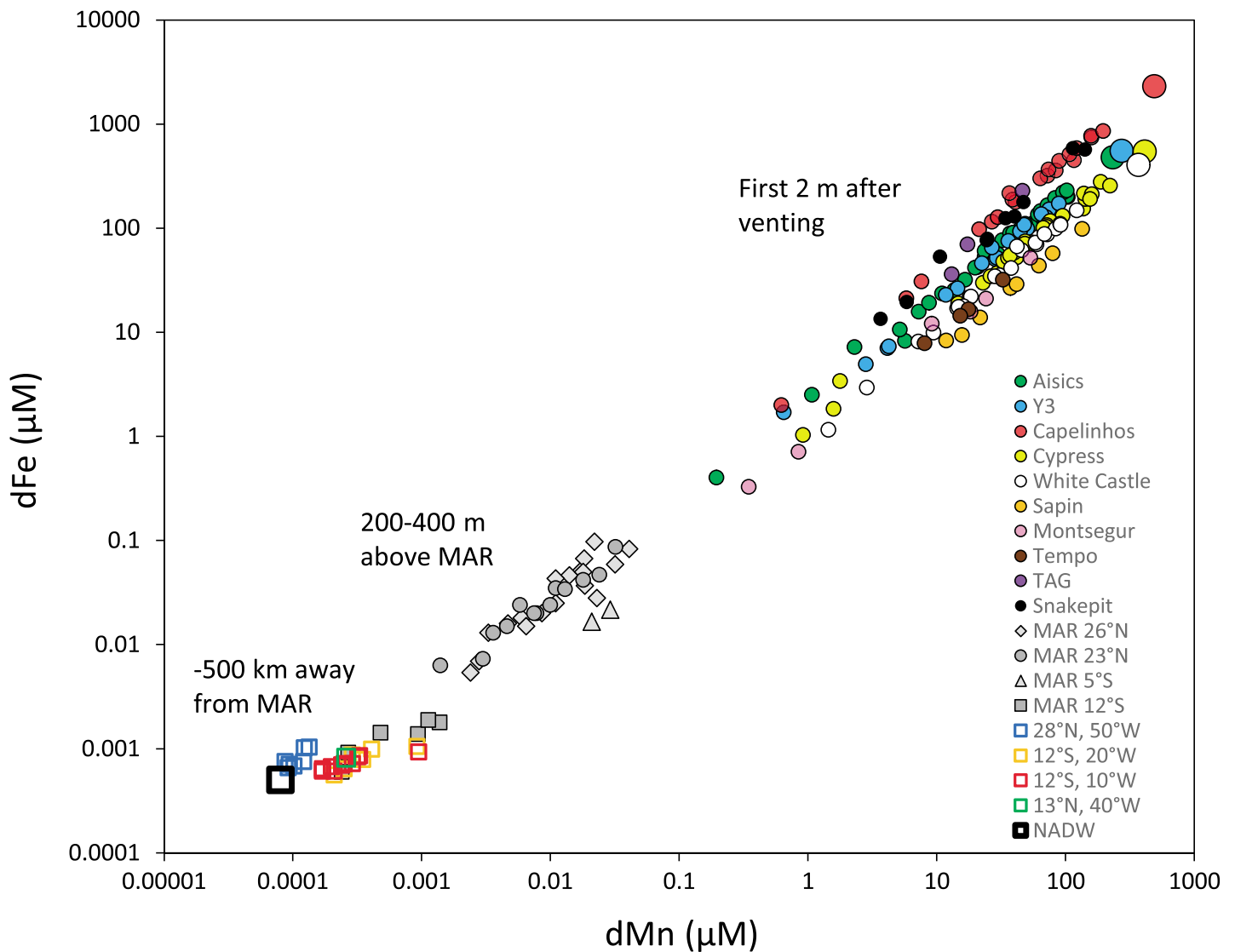


Figure 3. Dissolved Fe concentrations as a function of dissolved Mn concentrations along the continuum mixing gradient from hydrothermal solutions of the Mid-Atlantic Ridge (MAR) to North Atlantic Deep Waters (NADW). (from right to left) Hydrothermal solutions (bigger colored circles, our study); buoyant plumes in situ filtered at Lucky Strike (37°N), TAG (26°N), and Snakepit (23°N) fields (white and colored filled circles, our study); neutrally buoyant plumes 200–400 m above MAR at 26°N, 23°N, 5°S, and 12°S (grey filled symbols) [from references *James and Elderfield, 1996; Bennett et al., 2008; Saito et al., 2013; and Hatta et al., 2015*], water-column anomalies reported ~500 km away from MAR axis at 28°N and 12°S (colored open squares) [from references *Fitzsimmons et al., 2013; Saito et al., 2013; and Hatta et al., 2015*]. NADW indicates concentrations in the North Atlantic Deep Waters (seawater end-member) [from reference *Hatta et al., 2015*]. Note that different cutoffs were used to define the dissolved fraction in these studies, i.e., 0.2 μm [*Hatta et al., 2015*], 0.4 μm [*James and Elderfield, 1996; Bennett et al., 2008; Fitzsimmons et al., 2013; Saito et al., 2013*], and 0.45 μm (this study). However, very high consistency in dFe measurements is generally observed when these different pore sizes are compared [*Fitzsimmons and Boyle, 2012*].

Cu-bearing and Zn-bearing sulphide minerals precipitates and dominate at the earliest stage of buoyant plume formation. At the main smoker of Aisics, for example, particulate Cu and Zn (pZn and pCu, respectively) accounted for 95±6% and 85±23% of total Cu and Zn, respectively (Figure 2 and Table S3). This was corroborated by mineralogical observations of some filters, obtained after in situ filtration at Aisics, White Castle, and Capelinhos, which essentially showed the occurrence of sphalerite and chalcopyrite particles (E. Pelletier, personal communication). Interestingly, particulate iron (pFe) was observed at all sites at concentrations very close to that of pZn and pCu indicating a preferential coprecipitation of iron in mineral phases of high Cu and Zn content, as opposed to its precipitation as noncollomorphous pyrite. The atomic Fe content in chalcopyrite is ~30% (as for Cu) and can vary in the

range 10–20% in sphalerite [Hutchison and Scott, 1981]. We propose that the precipitation of Fe in the early stage of mixing is essentially limited to the inclusion of Fe in such phases. This constitutes an important limitation for the conversion of dissolved iron to particulate iron because concentrations of Zn and Cu in hydrothermal fluids are roughly two orders of magnitude below those of Fe.

3.4. Implications of Our Findings and New Constraints on the Fe Budget

In order to place our findings obtained at vent discharges in a more global perspective, we compared our dFe results with those reported in the water column above the MAR [James and Elderfield, 1996; Bennett et al., 2008; Saito et al., 2013; Hatta et al., 2015] and up to 500 km away from the ridge axis including recent GEOTRACES expeditions [Fitzsimmons et al., 2013; Saito et al., 2013; Hatta et al., 2015] (Figure 3). Dissolved manganese, whose removal rate is considerably slower than the emplacement of neutrally buoyant plumes, can be confidently used as a conservative tracer across a wide range of dilutions, i.e., until a dilution factor of $\sim 100,000$ (corresponding to dMn concentrations of $\sim 0.01 \mu\text{M}$) [Radford-Knoery et al., 1998]. For higher dilution factors, it only permits a comparison of the hydrothermal iron reactivity relative to that of manganese. Therefore, other conservative tracers, such as ^3He in excess, need to be used over basin-scale transport [Resing et al., 2015]. Nevertheless, our data sets bridge a gap between hydrothermal end-member and water column anomalies reported in neutrally buoyant plumes above the MAR (typically 200–400 m above hydrothermal discharge areas). Above TAG and Snakepit, the reported dissolved and particulate Fe concentrations [James and Elderfield, 1996; Hatta et al., 2015; Ohnemos and Lam, 2015] indicate that the neutrally buoyant plume is depleted by 15% and 25% in total Fe at TAG and Snakepit, respectively (see Table S2 for calculation details). This should represent a maximum value if considering the above mentioned mixing with secondary venting depleted in iron. Above TAG, Fe-hosted particles essentially consist in ferrihydrite, with no evidence for Fe-bearing sulfides [Ohnemos and Lam, 2015]. These data and observations above TAG and Snakepit are in line with our findings that a very small fraction of hydrothermal Fe ($<10\%$) is precipitated as sulfide. Oxidation of Fe(II) is thus the major mechanism to consider for hydrothermal iron removal, even for common basalt-hosted systems characterized by low Fe:H₂S ratios.

The global flux of hydrothermal Fe required to sustain the worldwide dissolved Fe distributions is $4.1 \pm 0.3 \text{ Gmol y}^{-1}$ [Resing et al., 2015]. Alternatively, German et al. [2015] estimated a Fe flux from focused hydrothermal venting in the range of $0.05\text{--}0.9 \text{ Gmol y}^{-1}$ and proposed that the remaining $3.2\text{--}4.05 \text{ Gmol y}^{-1}$ corresponds to diffuse hydrothermal venting. However, based on our data and those in the literature, we propose to reconsider the different ratios used by German et al. [2015] to estimate the flux from focused venting. This includes, for example, the assumption that 50% of hydrothermal Fe is rapidly removed as polymetallic sulfides in the initial stage of mixing as well as a very small fraction of Fe (i.e., $<1\%$) escapes pyrite precipitation at higher dilution by local deep water [Sander and Koschinsky, 2011]. Indeed, our data and other observations indicate that the removal of Fe in sulfidic minerals does not exceed 10% in the first meters of the buoyant plume and is below 20% at neutrally buoyant plumes such as TAG. In order to better constrain the processes controlling the dispersion of hydrothermal Fe in the water column, a future challenge is to study hydrothermal fields at larger scales, by taking into account the wide variety of emissions, i.e., focused and diffuse venting, and by acquiring data over the entire mixing gradient. In particular, we believe that the in situ filtration approach will be helpful to identify the processes acting within the poorly known upper part of the buoyant plume.

Acknowledgments

This letter is dedicated to the memory of our colleague and friend Benoît Pernet-Coudrier, who died tragically in January 2016. We thank the captains, crew of the Pourquoi Pas? and the Victor 600 ROV for their assistance at sea, Mathilde Cannat and Jérôme Blandin coordinators of the projects and cruises, Stefan Lalonde for comments, Rachael James for making available her data set, Nicolas Gayet for help in collecting the samples, Julie Tourolle for bathymetric map, Céline Liorzou, Marie-Laure Rouget, and Claire Bassoulet (PSO) for ICP-AES and ICP-MS measurements and to the two reviewers for their constructive comments and helpful suggestions on an earlier version of the manuscript. We acknowledge the financial support from the French ANR Luckyscales project (ANR-14-CE02-0008-02) and the EU project EMSO (<http://www.emso-eu.org/>). Supporting data are included as a table in the supporting information; any additional data may be obtained from M Waeles (e-mail: waeles@univ-brest.fr).

References

- Barreyre, T., J. Escartin, R. Garcia, M. Cannat, E. Mittelstaedt, and R. Prados (2012), Structure, temporal evolution, and heat flux estimates from the Lucky Strike deep-sea hydrothermal field derived from seafloor image mosaics, *Geochem. Geophys. Geosyst.*, *13*, Q04007, doi:10.1029/2011GC003990.
- Bennett, S. A., E. P. Achterberg, D. P. Connelly, P. J. Statham, G. R. Fones, and C. R. German (2008), The distribution and stabilisation of dissolved Fe in deep-sea hydrothermal plumes, *Earth Planet. Sci. Lett.*, *270*(3), 157–167.
- Besson, P., J. Degboe, B. Berge, V. Chavagnac, S. Fabre, and G. Berger (2014), Calcium, Na, K and Mg concentrations in seawater by inductively coupled plasma-atomic emission spectrometry: Applications to IAPSO seawater reference material, hydrothermal fluids and synthetic seawater solutions, *Geostand. Geoanal. Res.*, *38*(3), 355–362.
- Breier, J., B. Toner, S. Fakra, M. Marcus, S. White, A. Thurnherr, and C. German (2012), Sulfur, sulfides, oxides and organic matter aggregated in submarine hydrothermal plumes at 9° 50' N East Pacific Rise, *Geochim. Acta*, *88*, 216–236.
- Cotte, L., M. Waeles, B. Pernet-Coudrier, P.-M. Saradin, C. Cathalot, and R. D. Riso (2015), A comparison of in situ vs. ex situ filtration methods on the assessment of dissolved and particulate metals at hydrothermal vents, *Deep Sea Res., Part I*, *105*, 186–194.

- Feely, R. A., M. Lewison, G. J. Massoth, G. Robert-Baldo, J. W. Lavelle, R. H. Byrne, K. L. Von Damm, and H. C. Curl (1987), Composition and dissolution of black smoker particulates from active vents on the Juan de Fuca Ridge, *J. Geophys. Res.*, *92*(B11), 11,347–11,363, doi:10.1029/JB092iB11p11347.
- Field, M. P., and R. M. Sherrell (2000), Dissolved and particulate Fe in a hydrothermal plume at 9°45' N, East Pacific Rise: Slow Fe (II) oxidation kinetics in Pacific plumes, *Geochim. Cosmochim. Acta*, *64*(4), 619–628.
- Fitzsimmons, J. N., and E. A. Boyle (2012), An intercalibration between the GEOTRACES GO-FLO and the MITESS/Vanes sampling systems for dissolved iron concentration analyses (and a closer look at adsorption effects), *Limnol. Oceanogr. Methods*, *10*, 437–450.
- Fitzsimmons, J. N., R. Zhang, and E. A. Boyle (2013), Dissolved iron in the tropical North Atlantic Ocean, *Mar. Chem.*, *154*, 87–99.
- German, C., and K. Von Damm (2006), Hydrothermal processes, *Treatise Geochem.*, *6*, 181–222.
- German, C., A. Campbell, and J. Edmond (1991), Hydrothermal scavenging at the Mid-Atlantic Ridge: Modification of trace element dissolved fluxes, *Earth Planet. Sci. Lett.*, *107*(1), 101–114.
- German, C., L. Legendre, S. Sander, N. Niquil, G. Luther, L. Bharati, X. Han, and N. Le Bris (2015), Hydrothermal Fe cycling and deep ocean organic carbon scavenging: Model-based evidence for significant POC supply to seafloor sediments, *Earth Planet. Sci. Lett.*, *419*, 143–153.
- Graham, U., and H. Ohmoto (1994), Experimental study of formation mechanisms of hydrothermal pyrite, *Geochim. Cosmochim. Acta*, *58*(10), 2187–2202.
- Hatta, M., C. I. Measures, J. Wu, S. Roshan, J. N. Fitzsimmons, P. Sedwick, and P. Morton (2015), An overview of dissolved Fe and Mn distributions during the 2010–2011 US GEOTRACES north Atlantic cruises: GEOTRACES GA03, *Deep Sea Res., Part II*, *116*, 117–129.
- Hawkes, J. A., D. Connelly, M. Gledhill, and E. P. Achterberg (2013), The stabilisation and transportation of dissolved iron from high temperature hydrothermal vent systems, *Earth Planet. Sci. Lett.*, *375*, 280–290.
- Hutchison, M. N., and S. D. Scott (1981), Sphalerite geobarometry in the Cu-Fe-Zn-S system, *Econ. Geol.*, *76*(1), 143–153.
- James, R., and H. Elderfield (1996), Dissolved and particulate trace metals in hydrothermal plumes at the Mid-Atlantic Ridge, *Geophys. Res. Lett.*, *23*(23), 3499–3502, doi:10.1029/96GL01588.
- Jickells, T., Z. An, K. K. Andersen, A. Baker, G. Bergametti, N. Brooks, J. Cao, P. Boyd, R. Duce, and K. Hunter (2005), Global iron connections between desert dust, ocean biogeochemistry, and climate, *Science*, *308*(5718), 67–71.
- Klevenz, V., W. Bach, K. Schmidt, M. Hentscher, A. Koschinsky, and S. Petersen (2011), Geochemistry of vent fluid particles formed during initial hydrothermal fluid–seawater mixing along the Mid-Atlantic Ridge, *Geochem. Geophys. Geosyst.*, *12*, Q0AE05, doi:10.1029/2011GC003704.
- Lam, P. J., and J. K. Bishop (2008), The continental margin is a key source of iron to the HNLC North Pacific Ocean, *Geophys. Res. Lett.*, *35*, L07608, doi:10.1029/2008GL033294.
- Le Bris, N., P.-M. Sarradin, D. Birot, and A.-M. Alayse-Danet (2000), A new chemical analyzer for in situ measurement of nitrate and total sulfide over hydrothermal vent biological communities, *Mar. Chem.*, *72*(1), 1–15.
- Massoth, G. J., E. T. Baker, R. A. Feely, J. E. Lupton, R. W. Collier, J. F. Gendron, K. K. Roe, S. M. Maenner, and J. A. Resing (1998), Manganese and iron in hydrothermal plumes resulting from the 1996 Gorda Ridge Event, *Deep Sea Res., Part II*, *45*(12), 2683–2712.
- Mottl, M. J., and T. F. McConachy (1990), Chemical processes in buoyant hydrothermal plumes on the East Pacific Rise near 21°N, *Geochim. Cosmochim. Acta*, *54*(7), 1911–1927.
- Nishioka, J., H. Obata, and D. Tsumune (2013), Evidence of an extensive spread of hydrothermal dissolved iron in the Indian Ocean, *Earth Planet. Sci. Lett.*, *361*, 26–33.
- Ohnemus, D. C., and P. J. Lam (2015), Cycling of lithogenic marine particles in the US GEOTRACES North Atlantic transect, *Deep Sea Res., Part II*, *116*, 283–302.
- Radford-Knoery, J., J.-L. Charlou, J.-P. Donval, M. Aballea, Y. Fouquet, and H. Ondreas (1998), Distribution of dissolved sulfide, methane, and manganese near the seafloor at the Lucky Strike (37°17' N) and Menez Gwen (37°50' N) hydrothermal vent sites on the mid-Atlantic Ridge, *Deep Sea Res., Part I*, *45*(2), 367–386.
- Resing, J. A., P. N. Sedwick, C. R. German, W. J. Jenkins, J. W. Moffett, B. M. Sohst, and A. Tagliabue (2015), Basin-scale transport of hydrothermal dissolved metals across the South Pacific Ocean, *Nature*, *523*(7559), 200–203.
- Rickard, D. (1997), Kinetics of pyrite formation by the H₂S oxidation of iron (II) monosulfide in aqueous solutions between 25 and 125°C: The rate equation, *Geochim. Cosmochim. Acta*, *61*(1), 115–134.
- Rudnicki, M., and H. Elderfield (1993), A chemical model of the buoyant and neutrally buoyant plume above the TAG vent field, 26 degrees N, Mid-Atlantic Ridge, *Geochim. Cosmochim. Acta*, *57*(13), 2939–2957.
- Saito, M. A., A. E. Noble, A. Tagliabue, T. J. Goepfert, C. H. Lamborg, and W. J. Jenkins (2013), Slow-spreading submarine ridges in the South Atlantic as a significant oceanic iron source, *Nat. Geosci.*, *6*(9), 775–779.
- Sander, S. G., and A. Koschinsky (2011), Metal flux from hydrothermal vents increased by organic complexation, *Nat. Geosci.*, *4*(3), 145–150.
- Sarradin, P.-M., N. Le Bris, C. Le Gall, and P. Rodier (2005), Fe analysis by the ferrozine method: Adaptation to FIA towards in situ analysis in hydrothermal environment, *Talanta*, *66*(5), 1131–1138.
- Schoonen, M., and H. Barnes (1991), Mechanisms of pyrite and marcasite formation from solution: III. Hydrothermal processes, *Geochim. Cosmochim. Acta*, *55*(12), 3491–3504.
- Severmann, S., C. Johnson, B. Beard, C. German, H. Edmonds, H. Chiba, and D. Green (2004), The effect of plume processes on the Fe isotope composition of hydrothermally derived Fe in the deep ocean as inferred from the Rainbow vent site, Mid-Atlantic Ridge, 36°14'N, *Earth Planet. Sci. Lett.*, *225*(1), 63–76.
- Tagliabue, A. (2014), More to hydrothermal iron input than meets the eye, *Proc. Natl. Acad. Sci. U.S.A.*, *111*(47), 16641–16642.
- Tagliabue, A., L. Bopp, J.-C. Dutay, A. R. Bowie, F. Chever, P. Jean-Baptiste, E. Bucciarelli, D. Lannuzel, T. Remenyi, and G. Sarthou (2010), Hydrothermal contribution to the oceanic dissolved iron inventory, *Nat. Geosci.*, *3*(4), 252–256.
- Toner, B. M., S. C. Fakra, S. J. Manganini, C. M. Santelli, M. A. Marcus, J. W. Moffett, O. Rouxel, C. R. German, and K. J. Edwards (2009), Preservation of iron (II) by carbon-rich matrices in a hydrothermal plume, *Nat. Geosci.*, *2*(3), 197–201.
- Veirs, S. R., R. E. McDuff, and F. R. Stahr (2006), Magnitude and variance of near-bottom horizontal heat flux at the Main Endeavour hydrothermal vent field, *Geochem. Geophys. Geosyst.*, *7*, Q02004, doi:10.1029/2005GC000952.
- Vuillemin, R., D. Le Roux, P. Dorval, K. Bucas, J. Sudreau, M. Hamon, C. Le Gall, and P. Sarradin (2009), CHEMINI: A new in situ CHEMical MINIaturized analyzer, *Deep Sea Res., Part I*, *56*(8), 1391–1399.
- Wilson, C., J.-L. Charlou, E. Ludford, G. Klinkhammer, C. Chin, H. Bougault, C. German, K. Speer, and M. Palmer (1996), Hydrothermal anomalies in the Lucky Strike segment on the Mid-Atlantic Ridge (37°17'N), *Earth Planet. Sci. Lett.*, *142*(3), 467–477.
- Yücel, M., A. Gartman, C. S. Chan, and G. W. Luther III (2011), Hydrothermal vents as a kinetically stable source of iron-sulphide-bearing nanoparticles to the ocean, *Nat. Geosci.*, *4*(6), 367–371.